Baiu rainband termination in atmospheric and atmosphere-ocean models

Akira Kuwano-Yoshida[1]
Earth Simulator Center, Japan Agency for Marine-Earth Science and Technology, Yokohama, Kanagawa, Japan

Bunmei Taguchi
Earth Simulator Center, Japan Agency for Marine-Earth Science and Technology, Yokohama, Kanagawa, Japan

Shang-Ping Xie
International Pacific Research Center and the Department of Meteorology, University of Hawaii at Manoa, Honolulu, Hawaii, USA; Scripps Institution of Oceanography, University of California at San Diego, La Jolla, California, USA

[1] *Corresponding author address*: Akira Kuwano-Yoshida, Earth Simulator Center, Japan Agency for Marine-Earth Science and Technology, 3173-25, Showa-machi, Kanazawa-ku, Yokohama, Kanagawa, 236-0001, Japan.
E-mail: akiray@jamstec.go.jp

Abstract

Baiu rainband is a summer rainband stretching from eastern China through Japan towards the Northwest Pacific. The climatological termination of the Baiu rainband is investigated using Japanese 25-year ReAnalysis (JRA25), a stand-alone atmospheric general circulation model (GCM) forced with observed sea surface temperature (SST) and an atmosphere-ocean GCM (AOGCM). The Baiu rainband over the North Pacific abruptly shifts northward and weakens substantially in early July in the atmospheric GCM (AGCM), too early compared to observations (late July). The mid-troposphere westerly jet and its thermal advection explain this meridional shift of the Baiu rainband, but ocean surface evaporation modulates the precipitation intensity. In AGCM, deep convection in the subtropical Northwest Pacific sets in prematurely, displacing the westerly jet northward over cold ocean surface earlier than in observations. The suppressed surface evaporation over the cold ocean suppresses precipitation even though the mid-tropospheric warm advection and vertically integrated moisture convergence are similar to those before the westerly jet's northward shift. As a result, Baiu rainband abruptly weakens after the northward shift in JRA25 and AGCM. In AOGCM, cold SST biases in the subtropics inhibit deep convection, delaying the poleward excursion of the westerly jet. As a result, the upward motion induced by the strong westerly jet and the rainband both persist over the Northwest Pacific through summer in the AOGCM. Our results indicate that the westerly jet as well as ocean evaporation underneath are important for the Baiu rainband, the latter suggesting an oceanic effect on this important phenomenon.

1. Introduction

Baiu is a quasi-stationary rainband over East Asia and the Northwest Pacific in early summer between June and July, often characterized as a subtropical front in moisture between the tropics and extratropics (Ninomiya 1984; Ninomiya and Akiyama 1992). Baiu rainband shows multi-scale structures from meso- to synoptic scales (Ninomiya and Akiyama 1992). Because of the multi-scale nature, Baiu rainband provides much needed rainfall to supply precious water to a broad region of East Asia, causing local disasters such as floods and mudslides by heavy rain.

Recently Sampe and Xie (2010) proposed a hypothesis linking the subtropical jet and Baiu rainband. They suggest that horizontal warm advection by the subtropical jet induces upward motion in the middle troposphere using the thermodynamic energy equation. Specifically, the warm air mass over the Tibetan plateau flows westward on the upper jet over East Asia, and the adiabatic ascent on isentropic surfaces triggers convection in the Baiu rainband. Transient disturbances propagating from the Asian continent further aid convection along the jet. Latent heating within Baiu rainband modifies the upward motion strength. Kosaka et al. (2011) show that the hypothesis explains the interannual variability in Baiu rainband qualitatively.

Although much progress has been made in understanding Baiu rainband, several important questions remain. The seasonal termination of Baiu rainband is an unsolved issue. Baiu rainband gradually moves northward in mid-July, and abruptly terminates around late-July (Saito 1985; Sampe and Xie 2010). Saito (1985) suggested that weakening of the upper trough occurs at Baiu termination over Japan. Ueda et al. (1995) and Ueda and Yasunari (1996) proposed that “the subtropical convection jump” causes a Rossby wave train and triggers the abrupt Baiu termination. The subtropical convective jump is an abrupt northward shift of large-scale convective activity over the western Pacific around 20°N, 150°E in late July. In addition the shift is associated with tropical cyclone activity. The convective jump, however, does not appear clearly every year. Ueda and Ysunari (1996) reported that the typical convective jump rarely occurs in El-Nino years. While Ueda et al. (2009) suggest that atmospheric moistening may cause the subtropical convection jump rather than local SST, the mechanism has not been fully understood.

Another question is the origin of pronounced rainfall in the Baiu front. The moisture transport is considered important, by the southwesterly flow on the western flank of the North Pacific subtropical high and the westerly flow from the Bay of Bengal (Akiyama 1973; Kodama 1992). Matsumoto et al. (1971) suggest that the moisture transport from the south makes a larger contribution to precipitation over the East China Sea than over the Japan mainland. Since environment moisture influences the development of atmospheric disturbances in the Baiu front (Tochimoto and Kawano 2012), it is important to clarify the relative roles of local moisture supply (e.g. evaporation) and large-scale environmental transport in supporting Baiu rainband. Recent high-resolution observations of precipitation, sea surface temperature (SST) and surface winds from satellites provide more detailed structure of Baiu rainband. Sasaki et al. (2012) report that strong surface evaporation and surface convergence associated with local SST maximum along Kuroshio current strengthens Baiu precipitation over the East China Sea.

Atmospheric general circulation models (AGCMs) and atmosphere and ocean GCMs (AOGCMs) have been used to simulate and predict Baiu rainband. Ninomiya et al. (2002) report features of “Baiu phase” and “non Baiu phase” in an AGCM, suggesting that the upper jet, moisture flux and synoptic disturbances are important to reproduce the Baiu front even if continent-ocean thermal contrast is reasonably maintained in the model. Kawatani and Takahashi (2003) examine dependency on model resolution and cumulus parameterization of Baiu reproducibility in an AGCM. They suggest the importance of the subtropical jet strength and an early termination of the Baiu front in the AGCM regardless of cumulus parameterizations. Ninomiya (2009) reports large diversity of Baiu representation among current CGCMs in “the World Climate Research Programme’s Coupled Model Intercomparison Project phase 3” (CMIP3, Meehl et al. 2007). Although these studies note the importance of the subtropical jet for Baiu rainband maintenance, they do not offer specific mechanisms for this relationship.

The present study investigates the seasonal evolution of Baiu rainband using a reanalysis and a pair of AGCM and AOGCM. Each model shows a distinct seasonal march of Baiu rainband from the other, providing a unique opportunity to understand the mechanism of Baiu rainband maintenance and termination. We show that in both reanalysis and models, the seasonal march mostly follows that of the zonal jet through the mid-troposphere warm advection mechanism. The precipitation amount, however, corresponds less well with the warm advection forcing. The moisture budget analysis shows that local evaporation under and south of the Baiu rainband is important for the precipitation amount. After the Baiu termination, the northward shifted jet is located over cold sea surface temperature (SST) north of the Kuroshio-Oyashio extension, and weak evaporation from the sea surface reduces Baiu rainfall amount even though the mid-troposphere warm advection continues to force upward motion.

The rest of the paper is organized as follows. The description of the models and data are presented in Section 2, followed by an overview of Baiu seasonal march in the AGCM and observations (Section 3). Section 4 analyzes Baiu rainband termination, and Section 5 presents the moisture budget analysis of Baiu rainband. Section 6 discusses Baiu rainband mechanisms in the AOGCM, and Section 7 gives concluding remarks.

2. Data and methods

We use two models: the AGCM for the Earth Simulator version 3 (AFES; Ohfuchi et al. 2004, 2007; Enomoto et al. 2008; Kuwano-Yoshida et al. 2010), and the coupled atmosphere – ocean GCM for the Earth Simulator (CFES; Komori et al. 2008, Taguchi et al. 2012), which consists of AFES and the Coupled Ocean–Sea Ice Model for the ES (OIFES; Komori et al. 2005). AFES is based on the Center for Climate System Research/National Institute for Environmental Studies (CCSR/NIES) AGCM version 5.4.02 (Numaguti et al. 1997), while OIFES is based on the Modular Ocean Model version 3 (MOM3; Pacanowski and Griffies 2000). Computational codes of AFES and OIFES have been substantially rewritten from their prototypes, in order to attain their high computational efficiency on the particular architecture of ES and to implement improved parameterizations of physical processes. The models have medium horizontal resolution, T119 spectral truncation (equivalently 100-km grid intervals) with 48 levels for AFES, and 0.5^{o} grid intervals with 54 vertical levels for OIFES (Taguchi et al. 2012). The initial conditions of the atmosphere and ocean are climatology at 00UTC 1st January from the European Centre for Medium-Range Weather Forecasts (ECMWF) Re-Analysis (ERA40, Uppala et al. 2005) and the World Ocean Atlas 1998 (WOA98) (Antonov et al. 1998a, b, c; Boyer et al. 1998a, b, c) without motion, respectively. In this study, the first 20 years integration of the

CFES is used. Although CFES shows weak cooling drift in the first 5 years with a global mean surface temperature decrease of 0.5 K, it reaches a steady state after that and Baiu rainband remains steady through the first 20 years. AFES with the same resolution as CFES is integrated with the weekly NOAA Optimum Interpolation Sea Surface Temperature Analysis (OISST; Reynolds et al. 2002) from 1 September 1981 to 31 December 1999. The AFES data from 1 January 1982 is used in this study (AFES).

As observational reference, 6-hourly Japanese 25-year Reanalysis (JRA25; Onogi et al. 2007) is used from 1 January 1985 to 31 December 2004. The daily climatology data of model integrations and observations are used to investigate evolution of climatological Baiu rainband. To estimate precipitation associated with tropical cyclones, best track data from the Regional Specialized Meteorological Center (RSMC) Tokyo, Japan Meteorological Agency is used.

3. Overview of Baiu seasonal march

Figure 1 compares climatological Baiu rainband in June and July between JRA25, and AFES. In June, the Baiu rainband extends over south China through the southern coast of Japan to the northwestern Pacific Ocean in JRA25 (Fig. 1a). Precipitation is strong over south China, the East China Sea and southwest Japan, gradually weakening east of Japan over the Northwestern Pacific. AFES mostly reproduces the rainband, while it is located more north with weaker precipitation especially over sea than JRA25 (Fig. 1e). In the Baiu season, tropical cyclones contribute to rainfall in East Asia. Figure 1c shows precipitation without that associated with tropical cyclones. The precipitation associated with tropical cyclones is defined as precipitation inside of a circle where wind speed is 30 kt or greater by RSMC best track data. Although tropical cyclones affect precipitation over the Philippine Sea, the Baiu rainband is rarely influenced in June.

In July, AFES differs substantially from observations. In observations the Baiu rainband weakens and shifts northward, while precipitation over the subtropics east of the Philippines strengthens (Fig. 1b). The change in subtropics and midlatitude precipitation is connected with the Pacific Japan pattern (Ueda 1995). In AFES, subtropical convection expands too much northward and occupies the entire warm pool with SST > 28^{o}C whereas in JRA25, active convection is kept well south of the northern flank of the warm pool. Perhaps because of the excessive subtropical convection, the continuous mid-latitude rainband disappears. Over the Asian continent, rainfall shifts too far northward to cover the east Siberia (Fig. 1f). The weaker precipitation in the subtropics in AFES may be associated with weak tropical cyclone activity because of coarser resolution. In JRA25, tropical cyclones greatly contribute to precipitation over southern China, the East China Seas and southern coast of Japan (Fig. 1d). However, the contribution of tropical cyclones is weak to the Baiu rainband over east of Japan.

To examine the Baiu rainband over the Northwestern Pacific east of Japan, precipitation averaged between 140^{o}E and 170^{o}E with 5-day running mean is shown in Fig. 2. Note that the precipitation includes precipitation associated with tropical cyclones, though the tropical cyclone's influence is small in the area (Fig. 1). In JRA25, the Baiu rainband is located around 35^{o}N from May to late July, and suddenly weakens around late-July, while subtropical precipitation becomes active, as reported by Ueda et al. (1995) and Sampe and Xie (2010) (Fig. 2a). In AFES the rainband weakens and shifts northward at the beginning of July three weeks earlier than in

JRA25 (Fig. 2b). The onset of subtropical precipitation (15º – 25ºN) occurs concurrently with the Baiu termination.

Sampe and Xie (2010) propose that the horizontal warm temperature advection by the zonal jet in the mid-troposphere induces upward motion of the Baiu rainband. Here we test this hypothesis in the seasonal march of vertical motions, horizontal temperature advection and zonal wind at 500 hPa (Fig. 3). The upward motion band in AFES corresponds well with horizontal warm advection band, similar to JRA25 as suggested by Sampe and Xie (2010). The meridional migrations match one another among vertical velocity, warm advection and the westerly jet. During the northward migration, the upper jet weakens in JRA25 and AFES. These results suggest that the northward migration of Baiu rainband and resultant termination mostly depend on the westerly jet and horizontal temperature advection, confirming Sampe and Xie's hypothesis in the context of Baiu seasonal variation. However, the magnitude of upward motions and precipitation does not always agree with that of temperature advection.

4. Termination of Baiu rainband

In this section we focus on the Baiu termination to characterize the change before and after. Figure 4 shows 10-day mean fields of SLP and precipitation from 21 June to 30 June and from 21 July to 30 July, periods when the subtropical convection jump takes place in AFES and JRA25, respectively. In JRA25, the Baiu rainband is located on the north edge of the subtropical high over the Pacific before the Baiu termination (Fig. 4a). After the termination the rainband almost disappears and the subtropical ridge shrinks eastward associated with a precipitation increase in the subtropics while in the mid-latitudes, the ridge extends over the Sea of Okhotsk (Fig. 4b). In AFES the rainband near Japan is weaker than that in JRA25 before Baiu termination (Fig. 4c). The rainband disappears with a northward shift of the zonal ridge in July (Fig. 4d), associated with a too early onset of the subtropical convection (see Fig. 2b). The results are consistent with “the subtropical convective jump” of Ueda et al. (1995) and its effect on the Baiu rainband.

As a part of the Asian monsoon system, land-sea contrast is important for the Baiu rainband formation (Yoshikane et al. 2001). Figure 5 shows temperature and zonal wind at 500 hPa before and after the Baiu termination. As suggested by Sampe and Xie (2010) there is a warm region over the Tibetan Plateau and the zonal jet advects the warm temperature through south of Japan to the Northwestern Pacific before the Baiu termination in JRA25 (Fig. 5a). After the Baiu termination the zonal jet shifts northward and weakens (Fig. 5b). In AFES the temperature fields before and after the Baiu termination resemble JRA25. The westerly jet is too weak before the Baiu termination and shifts too much northward after the Baiu termination compared to JRA25 (Figs. 5c and 5d).

Under these large-scale environments, horizontal temperature advection and upward motion show sharp changes before and after the Baiu termination in JRA25 and AFES (Fig. 6). Before the Baiu termination they peak in a zonal band from south China to the southern coast of Japan and the Northwestern Pacific anchoring the Baiu rainband in JRA25 as suggested by Sampe and Xie (2010) (Figs. 6a and 4a). After the Baiu termination they weaken over southern China and the southern coast of Japan and horizontal warm advection is large over the northern Japan and the Northwestern Pacific (Fig. 6b). The AFES shows similar distributions and seasonal evolution to JRA25 with the band of maximum displaced northward due to the biases of the westerly jet (Figs. 6c and 6d). These results suggest that the general location and seasonal evolution of the Baiu rainband is consistent with the hypothesis by Sampe and Xie (2010). However, there are inconsistencies between warm advection, upward motion and precipitation in JRA25 and AFES. In late June the rainband and upward motion in JRA25 over the Northwestern Pacific are weaker than that over southern China and the southern coast of Japan (Fig. 4a) in spite of a similar magnitude in warm advection (Fig. 6a). In AFES, also, the warm advection remains strong and is organized into a zonal band over northern Japan and the Northwestern Pacific while rain and upward motion are disorganized and scattered at the end of July (Figs. 4d and 6d). These inconsistencies indicate other factors that contribute to precipitation amount and upward motion amplitude of the Baiu rainband. The SST frontal effect on convection has been documented along the Gulf Stream (Minobe et al. 2008 and 2010; Kuwano-Yoshida et al. 2010; Chelton and Xie 2010) and Kuroshio (Xu et al. 2011; Sasaki et al. 2012).

5. Moisture budget of Baiu rainband

The previous section suggested that the Baiu rainband strength cannot be fully explained by horizontal temperature advection in the mid-troposphere alone, although the meridional shift of the Baiu rainband is associated with the upper jet shift. Moisture budget analysis is useful to understand precipitation amount. The moisture budget equation can be written as follows:

$$\int_{250hPa}^{SLP} \frac{\partial q}{\partial t} dp = \int_{250hPa}^{SLP} -\nabla \cdot (q\mathbf{V}) dp + E - P \ , \qquad (1)$$

where q is the specific humidity, t the time, p the pressure, $\mathbf{V}$ the horizontal velocity, E surface evaporation and P precipitation. Because the left-hand side in Eq. 1 is negligible for the long term mean, the terms in the right-hand side are analyzed here.

Figure 7 shows the seasonal march of moisture budget over the Northwestern Pacific. The Baiu rainband mostly overlaps with the maximum of vertical integrated moisture convergence for JRA25 and AFES. As the Baiu rainband weakens and shifts northward in JRA25 and AFES, precipitation weakens considerably more than moisture convergence (Figs. 7a and 7c). The moisture convergence zone shifts northward to the north of the large meridional SST gradient zone (called the SST front, hereafter), where surface evaporation vanishes in JRA25 and AFES (Figs. 7b and 7d). Surface evaporation shows a sharp decrease across the SST front because the prevailing southwesterlies advect warm and humid air over the cold ocean surface, causing fog north of the SST front (Tokinaga et al. 2009). These results suggest that the SST modulation of surface evaporation contributes to the strength of Baiu rainband, while horizontal convergence associated with warm advection-induced upward motion sets the location of Baiu rainband .

In JRA25, during the Baiu season the band of moisture convergence forms over southern China, the East China Sea, southern Japan and east of Japan with the southwesterly moisture flux (Fig. 8a). Beneath the convergence zone, surface evaporation is large. After the Baiu rainband termination, the moisture convergence zone shifts north of 40°N where the SST front is located (Fig. 8b). Surface evaporation under the moisture convergence zone is nearly zero because of cold SST and moist air advection from south. As a result precipitation weakens. Precipitation is weak over the East China Sea in AFES during the Baiu season (Fig. 4c), While the upper warm advection is displaced north over the Yellow Sea (Fig. 6c) and large moisture flux flows into there from the tropics, the surface evapotarion is negative over the Yellow Sea and the East China Sea. In late July, the moisture convergence zone shifts the north of 40^{o}N where the surface evaporation is negative in AFES (Fig. 8d), resulting in a weak precipitation (Fig. 4c). The results support that upper-level warm advection controls precipitation location, while the precipitation amount depends on surface evaporation.

The moisture budget analysis shows that relative location of the Baiu rainband to the SST front affects the Baiu rainband strength before and after the Baiu termination. Since the timing of Baiu termination shows large interannual variations (Kosaka et al. 2011), a simple climatological average may not capture the Baiu termination characteristics. We use the maximum of horizontal tempareture advection at 500 hPa in 5-day running mean and zonal mean between 140^{o}E and 170^{o}E (TADV500) as an index of dynamical Baiu location for each year. The maximum is searched between 20^{o}N and 60^{o}N. Figure 9 shows the daily frequency of the TADV500 maximum as a function of time and latitude. The frequency = 1 means that the TADV500 has maximum at particular latitude at particular day in 1 day among 20 year. Note that the frequency is also operated by 5-day running mean. In JRA25 the frequency peak is consistent with the climatological maximum of TADV500 in Fig. 3c. A second peak appears from late June to the first half of July along 42^{o}N (Fig. 9a), associated with years with earlier Baiu termination than the climatology. In AFES, the double peaks are clear in June followed by the single peak in July (Fig. 9b).

To analyze relation between the dynamical Baiu location and the SST front, two composites relative to the latitude of TADV500 maximum are made: one is for the TADV500 maximum being located between 40^{o}N and 50^{o}N (called as N) and the other between 30^{o}N and 40^{o}N (S). The composites S and N correspond to the composites for the periods during and after the Baiu, respectively. Figure 10 shows N and S composites of the moisture budget equation averaged between 140^{o}E and 170^{o}E. The origin of the horizontal axis (0^o) indicates the TADV500 maximum. In the N composite, the precipitation peak under the TADV500 maximum is smaller than the moisture convergence peak (Fig. 10a). The residuum of moisture is explained by the moisture tendency term, the left-hand side of Eq. 1, associated with the seasonal transition (not shown). Evaporation is almost zero because of the SST front. In contrast, the precipitation peak is clear and as large as the moisture convergence under the TADV500 maximum in the S composite (Fig. 10b). Evaporation is large to the south of the TADV500 maximum where the moisture diverges. In the difference between S and N composites, the SST is higher under the TADV500 maximum in the S composite. The moisture convergence accounts for 2/3 of the precipitation difference and evaporation for 1/3. In addition evaporation south of the TADV500 maximum compensates the moisture divergence. Since southwesterly wind prevails there, the evaporated moisture is transported under the TADV500 maximum, maintaining the Baiu rainband.

Similar features can be seen in AFES. In the N composite, the moisture convergence shows a peak under the TADV500 maximum and the evaporation is almost zero there, while precipitation peak slightly shifts northward (Fig. 10d). In the S composite, the moisture convergence and evaporation maintain the large precipitation peak under the TADV500 maximum (Fig. 10e). The difference between S and N composites shows the moisture convergence and evaporation each contribute to a half of the precipitation difference, because evaporation under the TADV500 maximum is larger than JRA25 (Fig. 10f). These results suggest that the Baiu rainband is not only maintained by the dynamical forcing of horizontal temperature advection at the middle troposphere, but sea surface evaporation is also significant to maintain the Baiu rainband.

The Baiu rainband termination occurs when the TADV500 maximum shifts north of the SST front, where SST and the moisture supply from sea surface are both weak.

6. Baiu rainband in CFES

Previous section shows that the relative position of the TADV500 maximum to the SST front is important to the Baiu rainband maintenance and the Baiu termination. In this section, we focus on the Baiu rainband in CFES to understand what controls the Baiu rainband in GCMs. Figure 11 shows the Baiu's seasonal march over the North-western Pacific in CFES. The Baiu rainband continues from May to September over the SST front without the Baiu termination in contrast to JRA25 and AFES (Fig. 11a). While the TADV500 maximum gradually moves northward as in JRA25 and AFES, it never goes beyond 40^{o}N (Fig. 11b). The moisture budget analysis shows the rainband locates over the SST front and the moisture flux converges under the TADV500 maximum from south (Figs. 11c and 11d). These results suggest that the Baiu rainband in CFES continues without a clear termination because the TADV500 maximum stays over the warm side of the SST front, supported by large moisture supply from the sea surface.

The stagnation of TADV500 maximum in CFES may be caused by several mechanism. One is SST bias in CFES. The cold SST bias in the subtropics suppresses the subtropical convection jump, allowing only a weak northward migration of the mid-latitude jet (Fig. 11a). Okajima and Xie (2007) noted a similar evolution of SST anomalies and interaction with summer convection over the Northwest Pacific in response to orographic forcing by the Tibetan Plateau. Secondly, the cold SST bias is larger in higher latitudes, making a shaper SST front in mid-latitudes. The strong SST front anchors and strengthens the mid-latitude atmospheric jet. In a result, the warm advection by the mid-latitude jet cannot move northward across the SST front. These results suggest the importances of the westerly jet and SST for the Baiu rainband and subtropical convection in AOGCMs.

7. Summary and conclusions

We have compared the Baiu ranbands in JRA25 and a pair of AGCM and AOGCM that share the same atmospheric component. Compared to JRA25, the Baiu rainband terminates about one month early in AFES while it persists through the summer in CFES. The difference in the Baiu rainbands between AFES and CFES is closely tied to subtropical convection to the south, consistent with Ueda et al. (1995, 2009). Our analysis shows that the mid-tropospheric horizontal thermal advection mechanism of Sampe and Xie (2010) partly explains the Baiu termination in AFES and the lack of it in CFES. This mechanism alone is insufficient, and the rapid northward decrease in ocean evaporation across the mid-latitude SST front is necessary to account for the abrupt precipitation decrease along the westerly jet after the Baiu termination. CFES suffers large cold SST biases, which affect ocean evaporation, the position and intensity of the westerly jet, and thereby the Baiu rainband location and strength.

Based on the findings, we propose a conceptual model of the Baiu rainband termination as summarized in Fig. 12. During the Baiu season, the rainband is maintained by upward motion induced by mid-troposphere warm advection and surface evaporation south of the SST front (Fig. 12a). At the Baiu termination, the mid-troposphere jet shifts northward over the cold SST north of the SST front where surface evaporation is suppressed. Changes in moisture convergence are small before and after the Baiu termination. As a result, the rainband weakens due to decreased moisture supply despite upward motion induced by the band of mid-tropospheric warm temperature advection (Fig 12b). The northward shift of the westerly jet may be triggered by the onset of subtropical convection as in Ueda and Yasunari (1996). Our results illustrate that surface conditions as well as the mid-tropospheric jet are important for Baiu rainband.

Climate models perform poorly and show large disagreement among themselves in Baiu simulation (Ninomiya 2011). While Baiu's relationship to the upper jet has recently been discussed, few studies have examined surface evaporation near Baiu and its effect on the rainband. Our analysis and the conceptual model provide a useful framework to assess climate models and understand future changes in Baiu models project.

Acknowledgments

AFES and CFES integrations were performed on the Earth Simulator with support of JAMSTEC. This work is supported by the Japanese Ministry of Education, Culture, Sports, Science and Technology (MEXT) through a Grant-in-Aid for Scientific Research in Innovative Areas 2205 "Hot Spots in Climate System", the U.S. NSF and NASA.

References

Akiyama, T., 1973: The large-scale aspects of the characteristic features of the Baiu front. *Pap. Meteor. Geophys.*, **24**, 157–188.

Antonov, J. I., S. Levitus, T. P. Boyer, M. E. Conkright, T. O'Brien, and C. Stephens, 1998a: *World Ocean Atlas 1998, Vol. 1: Temperature of the Atlantic Ocean.* NOAA Atlas NESDIS 27, U.S. Government Printing Office, Washington, D.C.

Antonov, J. I., S. Levitus, T. P. Boyer, M. E. Conkright, T. O'Brien, and C. Stephens, 1998b: *World Ocean Atlas 1998, Vol. 2: Temperature of the Pacific Ocean.* NOAA Atlas NESDIS 28, U.S. Government Printing Office, Washington, D.C.

Antonov, J. I., S. Levitus, T. P. Boyer, M. E. Conkright, T. O'Brien, C. Stephens, and B. Trotsenko, 1998c: *World Ocean Atlas 1998, Vol. 3: Temperature of the Indian Ocean.* NOAA Atlas NESDIS 29, U.S. Government Printing Office, Washington, D.C.

Boyer, T. P., S. Levitus, J. I. Antonov, M. E. Conkright, T. O'Brien, and C. Stephens, 1998a: *World Ocean Atlas 1998, Vol. 4: Salinity of the Atlantic Ocean.* NOAA Atlas NESDIS 30, U.S. Government Printing Office, Washington, D.C.

Boyer, T. P., S. Levitus, J. I. Antonov, M. E. Conkright, T. O'Brien, and C. Stephens, 1998b: *World Ocean Atlas 1998, Vol. 5: Salinity of the Pacific Ocean.* NOAA Atlas NESDIS 31, U.S. Government Printing Office, Washington, D.C.

Boyer, T. P., S. Levitus, J. I. Antonov, M. E. Conkright, T. O'Brien, C. Stephens, and B. Trotsenko, 1998c: *World Ocean Atlas 1998, Vol. 6: Salinity of the Indian Ocean.* NOAA Atlas NESDIS 32, U.S. Government Printing Office, Washington, D.C.

Chelton, D.B., and S.-P. Xie, 2010: Coupled ocean-atmosphere interaction at oceanic mesoscales. *Oceanogr.*, **23**, 52-69.

Enomoto, T., A. Kuwano-Yoshida, N. Komori, and W. Ohfuchi, 2008: Description of AFES 2: Improvements for high-resolution and coupled simulations. *High Resolution Numerical Modelling of the Atmosphere and Ocean*, Eds. K. Hamilton and W. Ohfuchi, 77–97, Springer, New York.

Fu, X., B. Wang, and T. Li, 2002: Impacts of air – sea coupling on the simulation of mean Asian summer monsoon in the ECHAM4 Model. *Mon. Wea. Rev.*, **130**, 2889–2904.

Inatsu, M., and M. Kimoto, 2005: Difference of boreal summer climate between coupled and atmosphere-only GCMs. *SOLA*, **1**, 105–108, doi:10.2151/sola.

Kanamitsu, Masao, Wesley Ebisuzaki, Jack Woollen, Shi-Keng Yang, J. J. Hnilo, M. Fiorino, G. L. Potter, 2002: NCEP–DOE AMIP-II Reanalysis (R-2). *Bull. Amer. Meteor. Soc.*, **83**, 1631–1643.

Kawase, H., T. Yoshikane, M. Hara, F. Kimura, T. Yasunari, B. Ailikun, H. Ueda, and T. Inoue, 2009: Intermodel variability of future changes in the Baiu rainband estimated by the pseudo global warming downscaling method. *J. Geophys. Res.*, **114**, 1–14.

Kawatani, Y., and M. Takahashi, 2003: Simulation of the Baiu front in a high resolution AGCM. *J. Meteor. Soc. Japan*, **81**, 113–126.

Kitoh, A., and O. Arakawa, 1999: On overestimation of tropical precipitation by an atmospheric GCM with prescribed SST. *Geophys. Res. Lett.*, **26**, 2965–2968.

Kodama, Y., 1992: Large-scale common features of subtropical precipitation zones (the Baiu frontal zone, the SPCZ, and the SACZ) Part I: Characteristics of subtropical frontal zones. *J. Meteor. Soc. Japan*, **70**, 813-836.

Komori, N., K. Takahashi, K. Komine, T. Motoi, X. Zhang, and G. Sagawa, 2005: Description of sea-ice component of coupled ocean – sea-ice model for the Earth Simulator (OIFES). *J. Earth Simulator*, **4**, 31–45.

Komori, N., A. Kuwano-Yoshida, T. Enomoto, H. Sasaki, and W. Ohfuchi, 2008: High-resolution simulation of global coupled atmosphere–ocean system: Description and preliminary outcomes of CFES (CGCM for the Earth Simulator). In *High Resolution Numerical Modelling of the Atmosphere and Ocean*, K. Hamilton and W. Ohfuchi (eds.), chapter 14, pp. 241–260, Springer, New York.

Kosaka, Y., S.-P. Xie, and H. Nakamura, 2011: Dynamics of Interannual Variability in Summer Precipitation over East Asia. *J. Climate*, **24**, 5435–5453.

Kusunoki, S., J. Yoshimura, H. Yoshimura, and A. Noda, 2006: Change of Baiu rain band in global warming projection by an atmospheric general circulation model with a 20-km grid size. *J. Meteor. Soc. Japan*, **84**, 581–611.

Kusunoki, S., R. Mizuta, and M. Matsueda, 2011: Future changes in the East Asian rain band projected by global atmospheric models with 20-km and 60-km grid size. *Climate Dyn.*, **37**, 2481–2493.

Kuwano-Yoshida, A., T. Enomoto, and W. Ohfuchi, 2010: An improved PDF cloud scheme for climate simulations. *Quart. J. Roy. Meteor. Soc.*, **136**, 1583–1597.

Kuwano-Yoshida, A., S. Minobe, and S.-P. Xie, 2010: Precipitation response to the Gulf Stream in an atmospheric GCM. *J. Climate*, **23**, 3676-3698.

Matsumoto, S., K. Ninomiya, and S. Yoshizumi, 1971: Characteristic features of ‘‘Baiu’’ front associated with heavy rainfall. *J. Meteor. Soc. Japan*, **49**, 267–281.

Meehl, G. a., C. Covey, K. E. Taylor, T. Delworth, R. J. Stouffer, M. Latif, B. McAvaney, and J. F. B. Mitchell, 2007: THE WCRP CMIP3 Multimodel Dataset: A New Era in Climate Change Research. *Bull. Amer. Meteor. Soc.*, **88**, 1383–1394.

Minobe, S., A. Kuwano-Yoshida, N. Komori, S.-P. Xie, and R. J. Small, 2008: Influence of the Gulf Stream on the troposphere. *Nature*, **452**, 206–209.

Minobe, S., M.Miyashita,A. Kuwano-Yoshida, H. Tokinaga, and S.-P. Xie, 2010: Atmospheric response to the Gulf Stream: Seasonal variations. *J. Climate*, **23**, 3699–3719.

Ninomiya, K., 1984: Characteristics of Baiu Front as a Predominant subtropical front in the summer Northern Hemisphere. *J. Meteor. Soc. Japan*, **62**, 880–894.

Ninomiya, K., 2009: Characteristics of Precipitation in the Meiyu-Baiu Season in the CMIP3 20th Century Climate Simulations. *J. Meteor. Soc. Japan*, **87**, 829–843.

Ninomiya, K., 2011: Characteristics of the Meiyu and Baiu Frontal Precipitation Zone in the CMIP3 20th Century Simulation and 21st Century Projection. *J. Meteor. Soc. Japan*, **89**, 151–159.

Ninomiya, K., and T. Akiyama, 1992: Multi-scale features of Baiu, the summer monsoon over Japan and the East Asia. *J. Meteor. Soc. Japan*, **70**, 467–495.

Ninomiya, K., T. Nishimura, W. Ohfuchi, T. Suzuki, and S. Matsumura, 2002: Features of the Baiu front simulated in an AGCM (T42L52). *J. Meteor. Soc. Japan*, **80**, 697–716.

Numaguti, A., M. Takahashi, T. Nakajima, and A. Sumi, 1997: Description of CCSR/NIES Atmospheric General Circulation Model. National Institute for Environmental Studies, Center for Global Environmental Research Supercomputer Monograph Rep. 3, 91 pp.

Ohfuchi, W. and Coauthors, 2004: 10-km mesh meso-scale resolving simulations of the global atmosphere on the Earth Simulator: Preliminary outcomes of AFES (AGCM for the Earth Simulator. *J. Earth Simulator*, **1**, 8–34.

Okajima, H., and S.-P. Xie, 2007: Orographic Effects on the Northwestern Pacific Monsoon: Role of Air-Sea Interaction. *Geophys. Res. Lett*., **34**, L21708, doi:10.1029/2007GL032206.

Onogi, K., and Coauthors, 2007: The JRA-25 reanalysis. *J. Meteor. Soc. Japan,* **85**, 369–432.

Pacanowski, R. C., and S. M. Griffies, 2000: Mom 3.0 Manual. Tech. Rep., Geophysical 1063 Fluid Dynamics Laboratory/National Oceanic and Atmospheric Administration, 680pp.

Reynolds, R.W., N.A. Rayner , T.M. Smith, D.C. Stokes, and W. Wang, 2002: An improved in situ and satellite SST analysis for climate. *J. Climate*, **15**, 1609–1625.

Saito, N., 1985: Quasi-stationary waves in mid-latitudes and the Baiu in Japan. *J. Meteor. Soc. Japan*, **63**, 983–995.

Sampe, T., and S.-P. Xie, 2010: Large-Scale Dynamics of the Meiyu-Baiu Rainband: Environmental Forcing by the Westerly Jet. *J. Climate*, **23**, 113–134.

Sasaki, Y. N., S. Minobe, T. Asai, M. Inatsu, 2012: Influence of the Kuroshio in the East China Sea on the Early Summer (Baiu) Rain. *J. Climate*, **25**, 6627–6645.

Taguchi, B., H. Nakamura, M. Nonaka, N. Komori, A. Kuwano-Yoshida, K. Takaya, and A. Goto, 2012: Seasonal Evolutions of Atmospheric Response to Decadal SST Anomalies in the North Pacific Subarctic Frontal Zone: Observations and a Coupled Model Simulation. *J. Climate*, **25**, 111–139.

Tochimoto, E. and T. Kawano 2012: Development Processes of Baiu Frontal Depressions. *SOLA*, **8**, 9-12.

Tokinaga, H., Y. Tanimoto, S.-P. Xie, T. Sampe, H. Tomita, and H. Ichikawa, 2009: Ocean frontal effects on the vertical development of clouds over the western North Pacific: In situ and satellite observations. *J. Climate*, 22, 4241-4260.

Ueda, H., T. Yasunari, and R. Kawamura, 1995: Abrupt seasonal change of large-scale convective activity over the western Pacific in the northern summer. *J. Meteor. Soc. Japan*, **73**, 795–809.

Ueda, H. and T. Yasunari, 1996: Maturing process of the summer monsoon over the western North Pacific – a coupled ocean/atmosphere system. *J. Meteor. Soc. Japan*, **74**, 493-508.

Ueda, H., M. Ohba, and S.-P. Xie, 2009: Important factors for the development of the Asian–Northwest Pacific summer monsoon. *J. Climate*, **22**, 649–669.

Uppala, S. M., P. W. K˚allberg, A. J. Simmons, U. Andrae, V. da Costa Bechtold, M. Fiorino, J. K. Gibson, J. Haseler, A. Hernandez, G. A. Kelly, X. Li, K. Onogi, S. Saarinen, N. Sokka, R. P. Allan, E. Andersson, K. Arpe, M. A. Balmaseda, A. C. M. Beljaars, L. van de Berg, J. Bidlot, N. Bormann, S. Caires, F. Chevallier, A. Dethof, M. Dragosavac, M. Fisher, M. Fuentes, S. Hagemann, E. H´olm, B. J. Hoskins, L. Isaksen, P. A. E. M. Janssen, R. Jenne, A. P. McNally, J.-F. Mahfouf, J.-J. Morcrette, N. A. Rayner, R.W. Saunders, P. Simon, A. Sterl, K. E. Trenberth, A. Untch, D. Vasiljevic, P. Viterbo, and J.Woollen, 2005: The ERA-40 re-analysis. *Quart. J. Roy. Meteor. Soc.*, **131**, 2961–3012.

Xu, H., M. Xu, S.-P. Xie, and Y. Wang, 2011: Deep atmospheric response to the spring Kuroshio Current over the East China Sea. *J. Climate*, 24, 4959-4972.

Yoshikane, T., F. Kimura, and S. Emori, 2001: Numerical study on the Baiu front genesis by heating contrast between land and ocean. *J. Meteor. Soc. Japan*, **79**, 671–686.

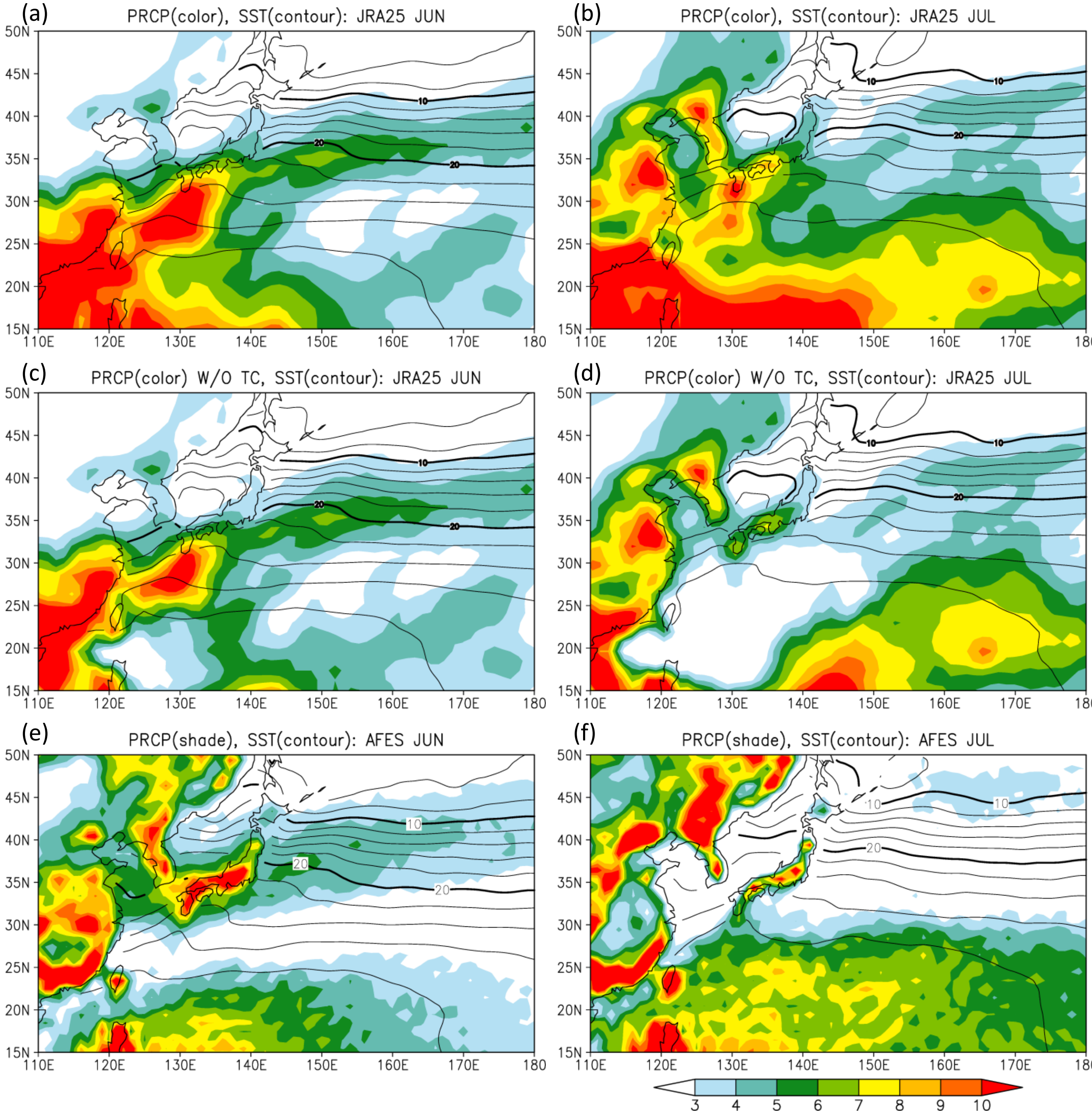

FIG. 1. Climatological precipitation (color, mm day^{-1}) and SST (contour interval is 2 ^{o}C with 10 ^{o}C and 20 ^{o}C thickened) in June (left) and July (right): (a) (b) JRA25, (c) (d) JRA25 without precipitation associated with tropical cyclones and (e) (f) AFES.

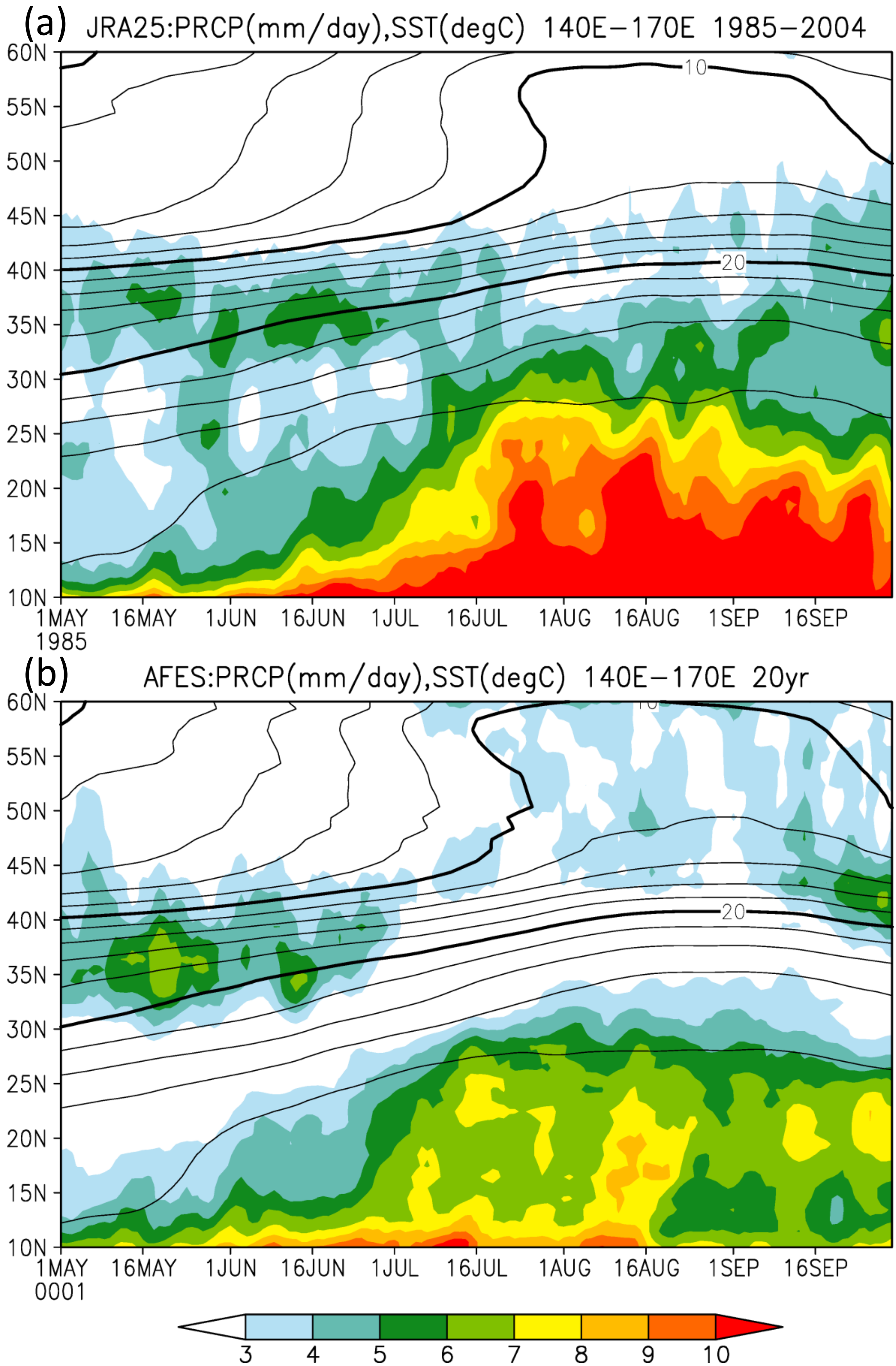

FIG. 2. Daily climatology of precipitation (color, mm day^{-1}) and SST (contour interval is 2 ^{o}C with 10 ^{o}C and 20 ^{o}C thickened) averaged between 140^{o}E and 170^{o}E with 5-day running mean of (a) JRA25 and (b) AFES from 1 May to 30 Sep.

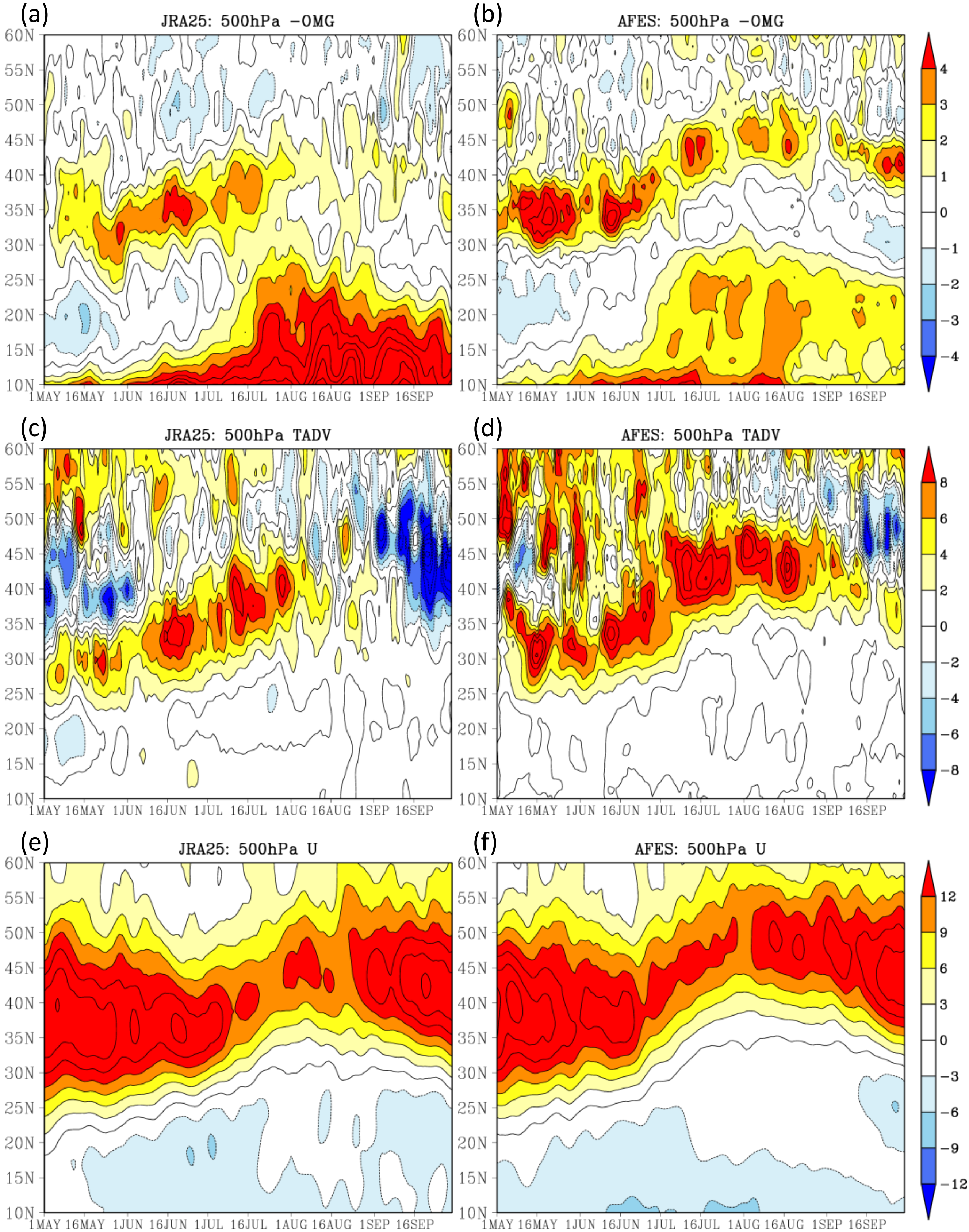

FIG. 3. As in Fig. 2 but for (a) (b) vertical pressure velocity with negative sign (10^{-2} Pa s^{-1}), (c) (d) horizontal temperature advection (10^{-6} K s^{-1}) and (e) (f) zonal wind (m s^{-1}) at 500 hPa: (left) JRA25 and (right) AFES.

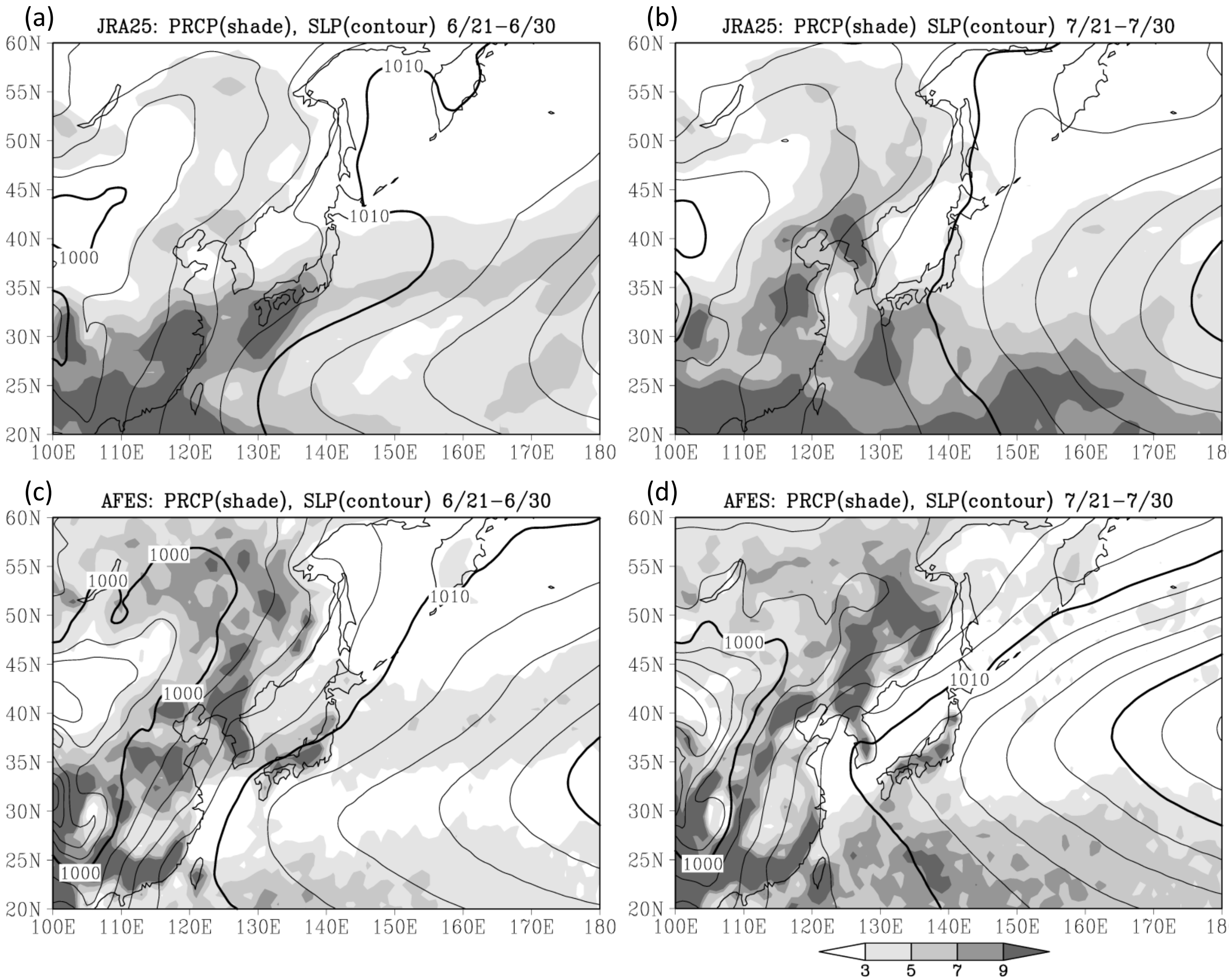

FIG. 4. 10-day mean of precipitation (shaded, mm day^{-1}) and SLP (contour interval is 2 hPa with 1000 hPa, 1010 hPa and 1020 hPa thickened) between (left) 21 June and 30 June, (right) 21 July and 30 July: (a) (b) JRA25 and (c) (d) AFES.

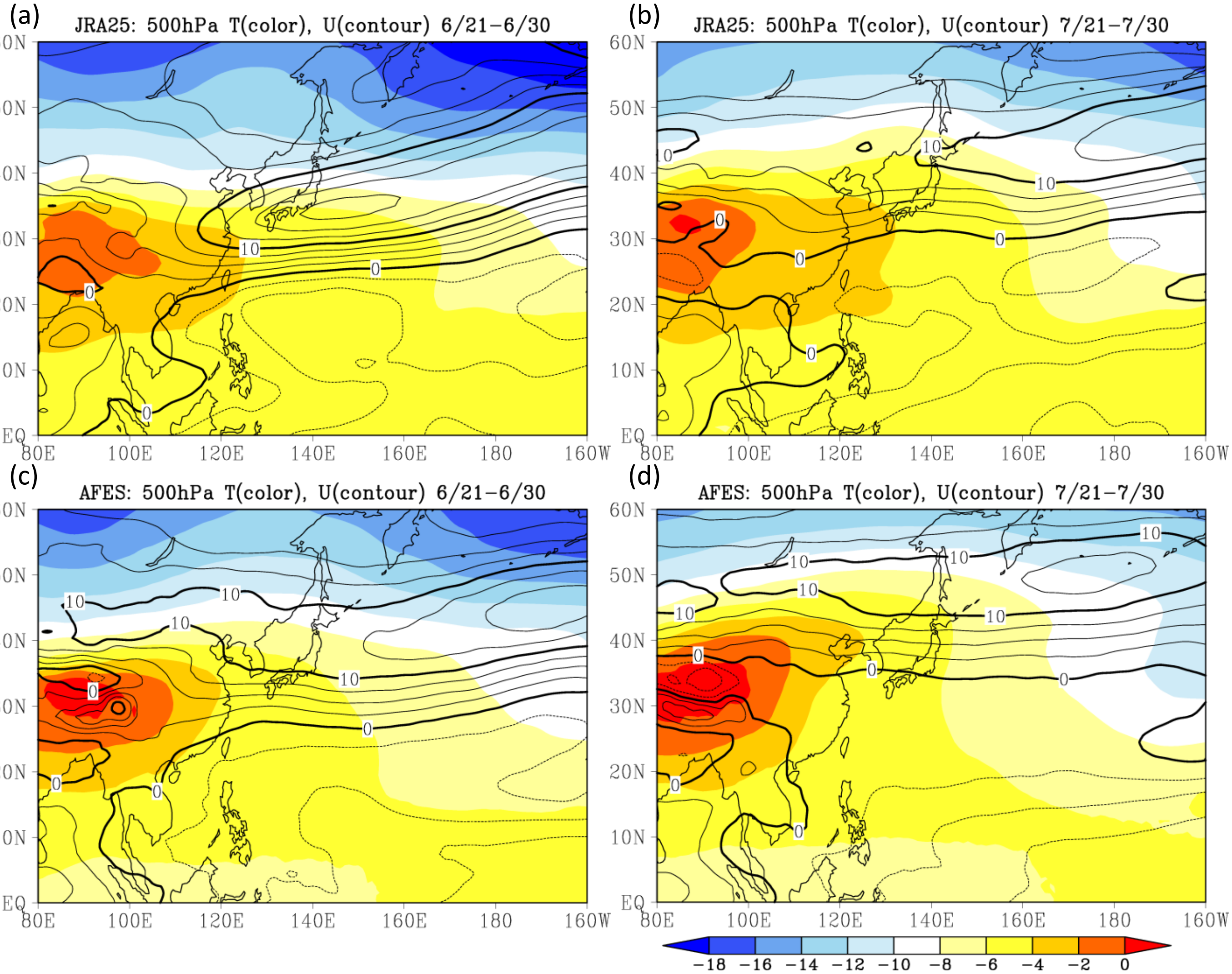

FIG. 5. As in Fig. 4 but for temperature (color, °C) and zonal wind (contour interval is 2.5 m s^{-1} with 0, 10, and 20 m s^{-1} thickened) at 500 hPa.

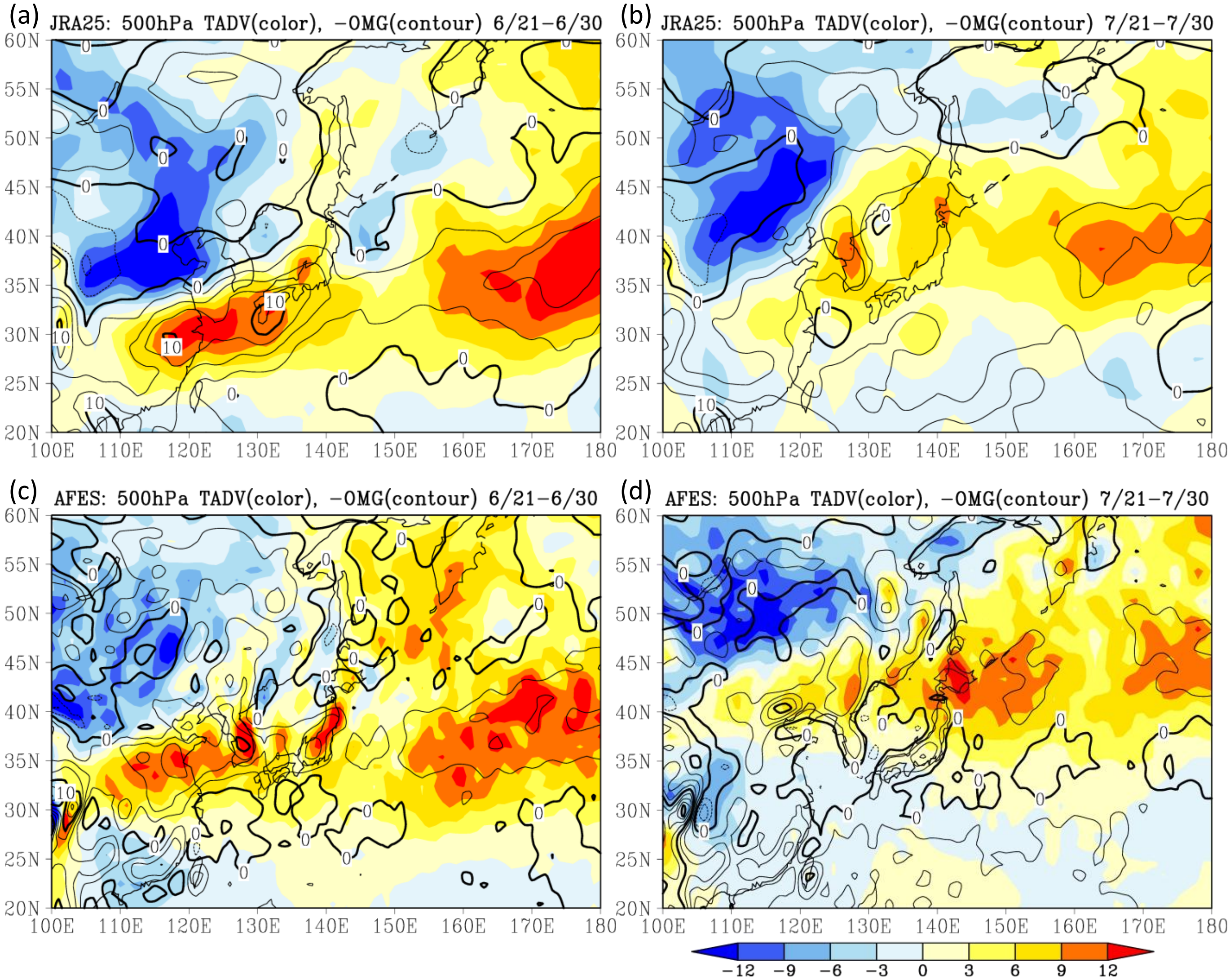

FIG. 6. As in Fig. 4 but for horizontal temperature advection (color, 10^{-6} K s^{-1}) and vertical p-velocity with negative sign (contour interval is 2.5 x 10^{-2} Pa s^{-1} with 0 and 10 x 10^{-2} Pa s^{-1} thickened) at 500 hPa.

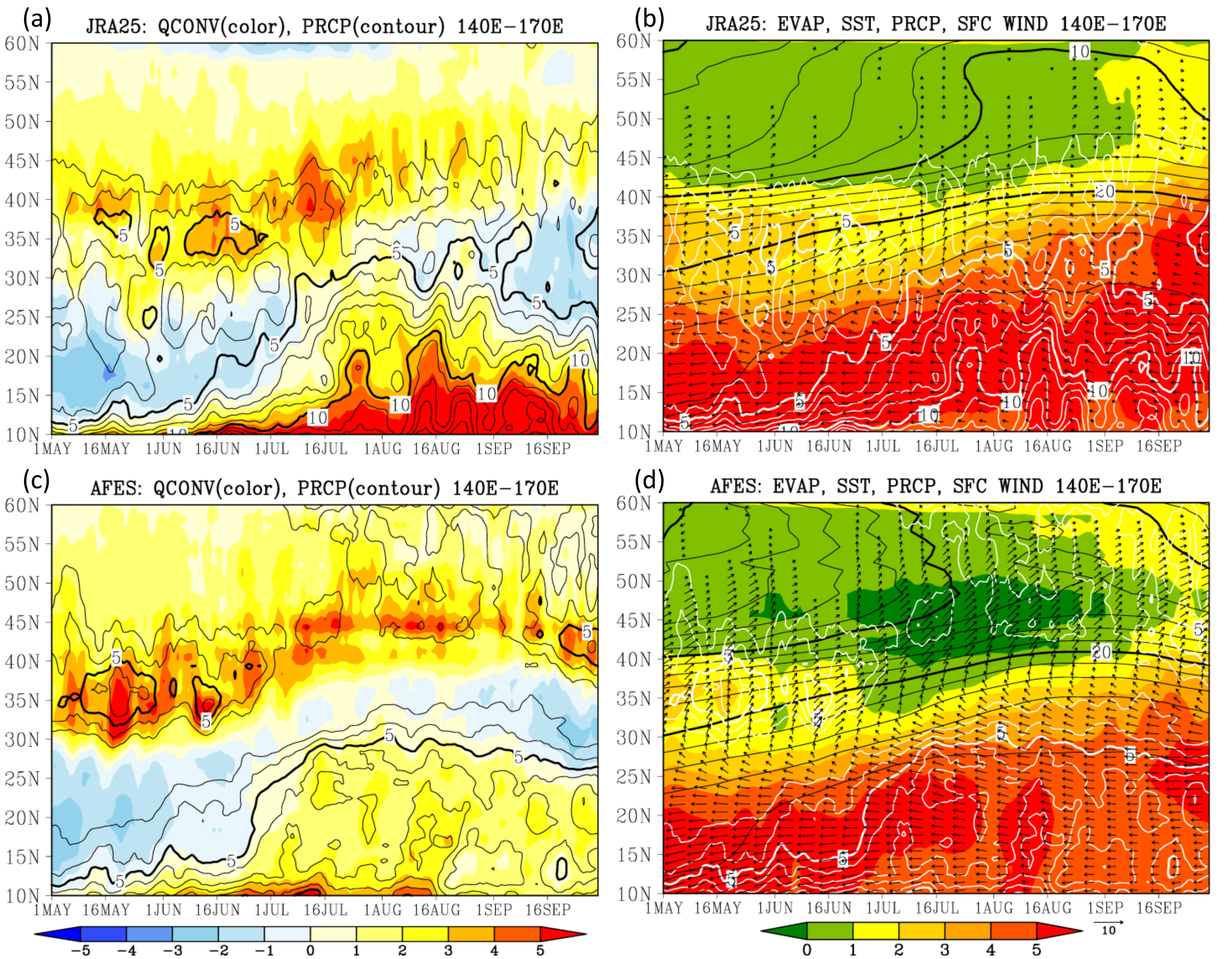

FIG. 7. As in Fig. 2, but for (left) vertical integrated moisture convergence from surface to 250 hPa (color, mm day^{-1}) and precipitation (contours are drawn for the range over 3 mm day^{-1} at every 1 mm day^{-1} with 5 mm day^{-1} and 10 mm day^{-1} thickened), (right) surface evaporation (color, mm day^{-1}), SST (black contour, contour interval is 2 °C with 10 °C and 20 °C thickened) surface wind (vector, m s^{-1}) and precipitation (white contours for the range over 3 mm day^{-1} at every 1 mm day^{-1} with 5 and 10 mm day^{-1} thickened): (a) (b) JRA25 and (c) (d) AFES.

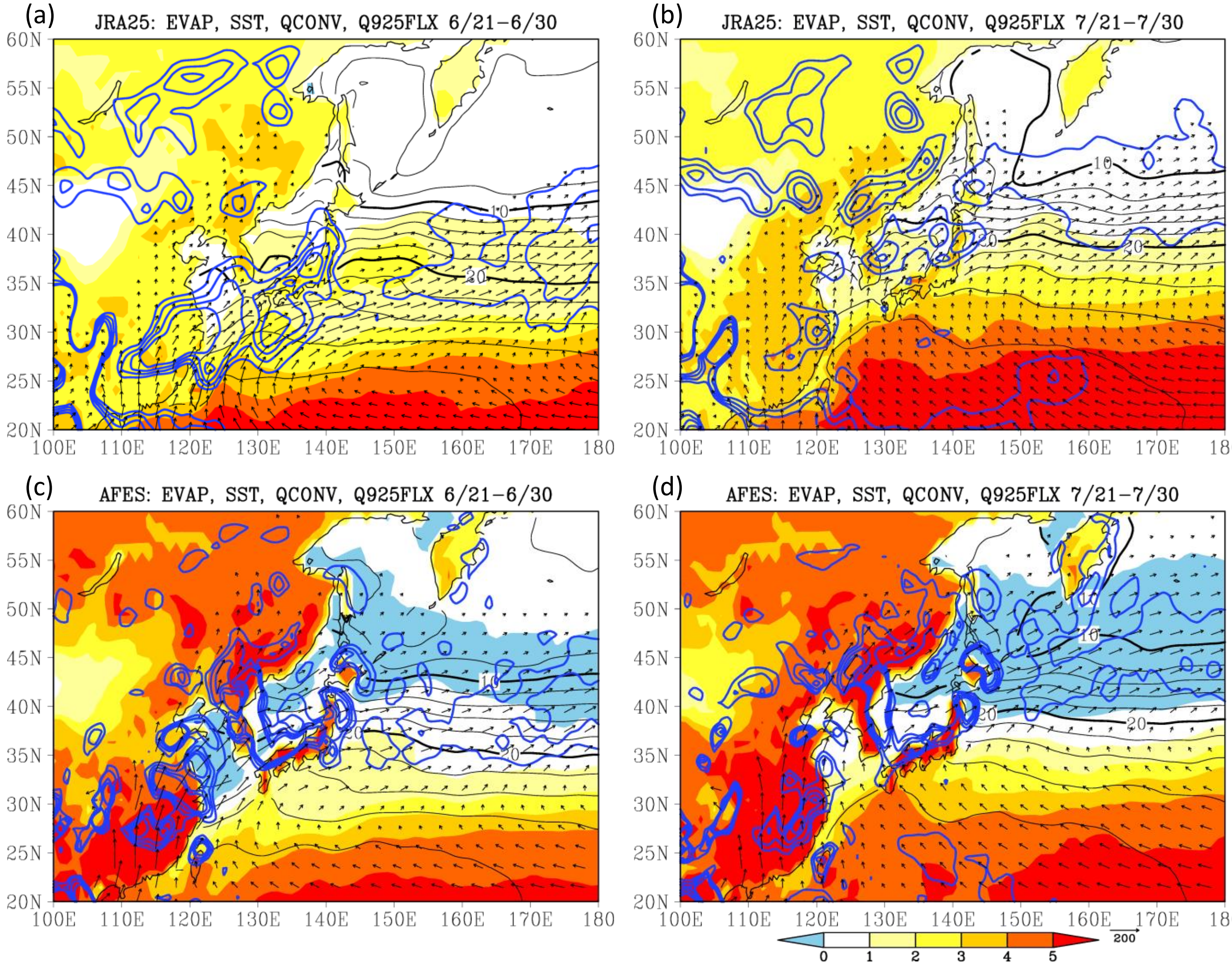

FIG. 8. As in Fig 4, but for surface evaporation (color, mm day-1), SST (black contour, contour interval is 2 ^{o}C with 10 ^{o}C and 20 ^{o}C thickened), moisture flux at 925 hPa (vector over 20 kg kg $^{-1}$ m s^{-1}) and vertically integrated moisture convergence (3, 5, 7, and 9 mm day^{-1} are plotted with blue contours).

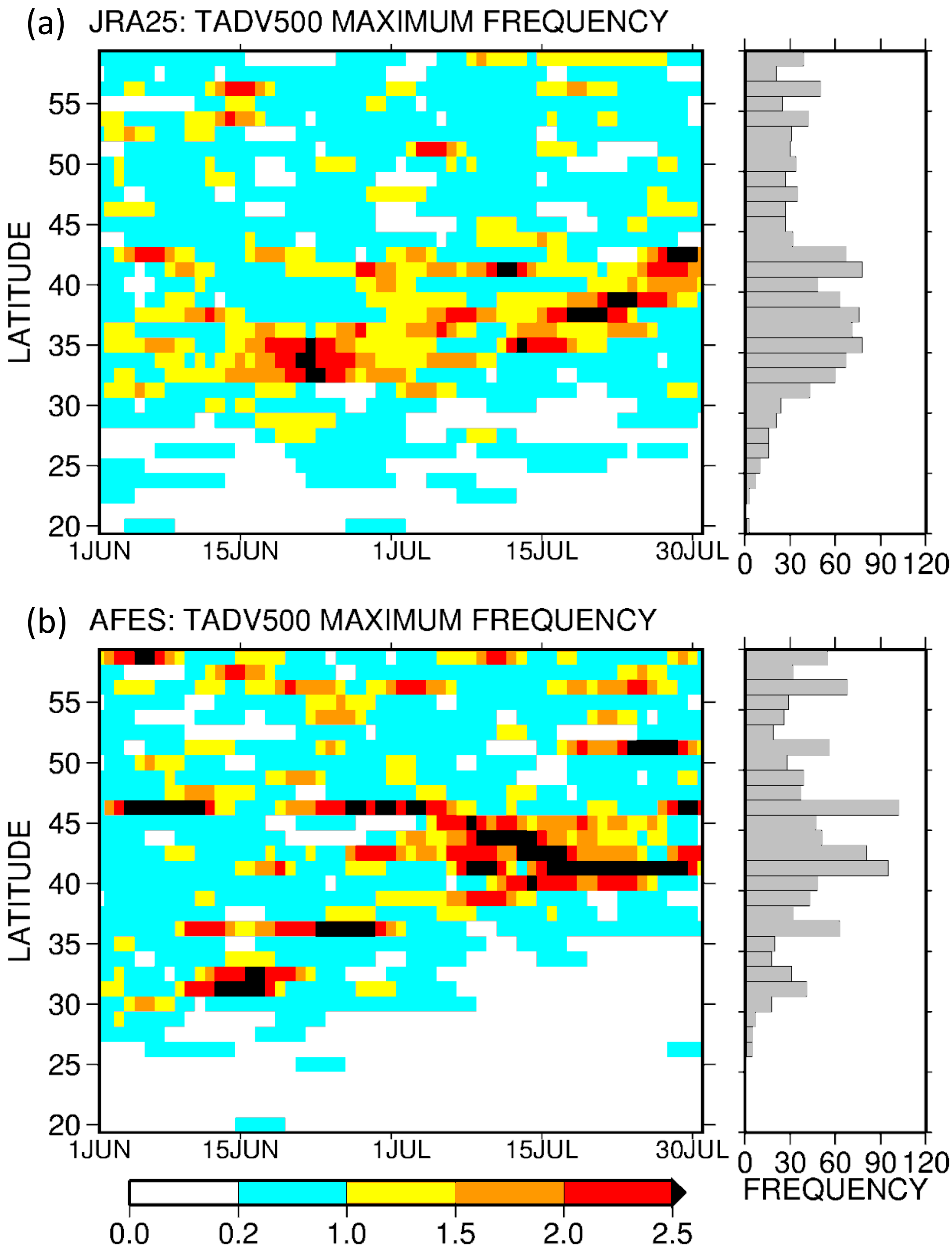

FIG. 9. (left) Daily appearance frequency of 500 hPa horizontal temperature advection maximum (detail definition is described in text) between 1 June and 31 July (color, 20 yr^{-1}) and (right) its cumulated frequency in June and July. (a) JRA25 (b) AFES.

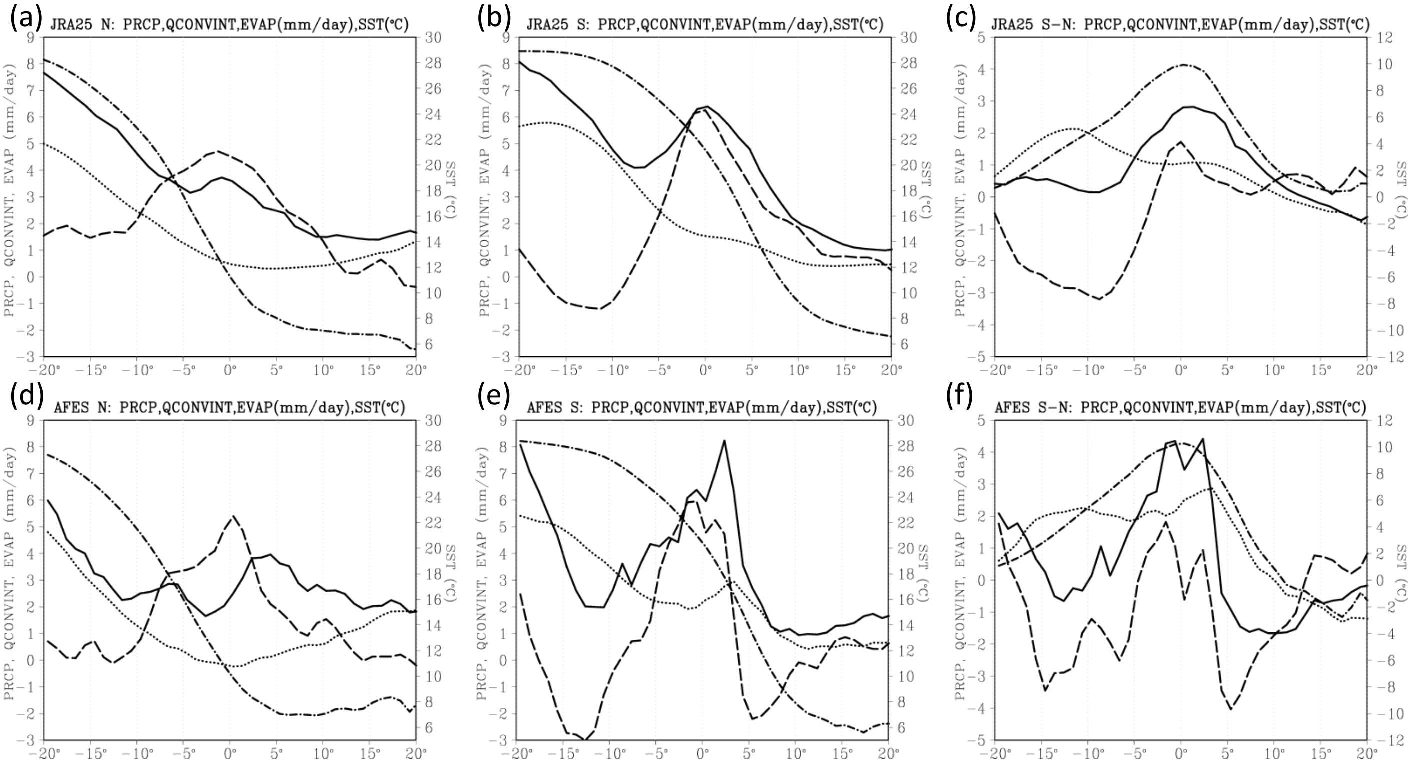

FIG. 10. Moisture budget analysis averaged between 140°E and 170°E for (a-c) JRA25 and (d-f) AFES. (a) (d) Composites when horizontal temperature advection maximum at 500 hPa is located between 40°N and 50°N (N), (b) (e) between 30°N and 40°N (S) and (c) (f) difference between S and N. Precipitation (mm day^{-1}, solid line), vertical integrated horizontal moisture convergence (mm day^{-1}, broken line), surface evaporation (mm day^{-1}, dotted line) and SST (°C, dotted – broken line, right axis).

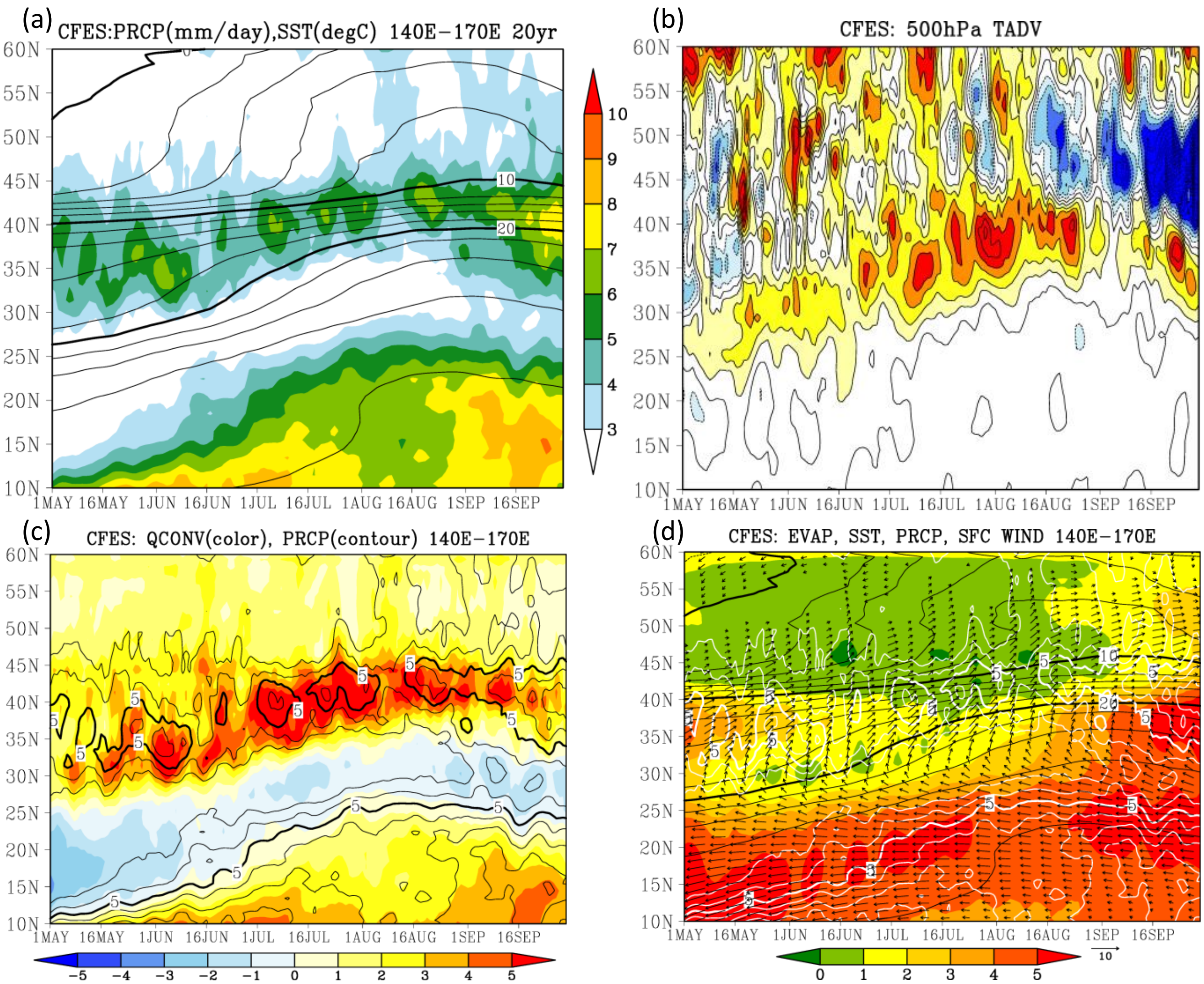

FIG. 11. Seasonal evolution of Baiu rainband in CFES. (a) precipitation (color, mm day^{-1}) and SST (contour interval is 2 ^{o}C with 10 ^{o}C and 20 ^{o}C thickened) averaged between 140^{o}E and 170^{o}E with 5-day running mean from 1 May to 30 Sep, (b) horizontal temperature advection at 500 hPa (10^{-6} K s^{-1}), (c) vertical integrated moisture convergence from surface to 250 hPa (color, mm day^{-1}) and precipitation (contours are drawn for the range over 3 mm day^{-1} at every 1 mm day^{-1} with 5 mm day^{-1} and 10 mm day^{-1} thickened) and (d) surface evaporation (color, mm day^{-1}), SST (black contour, contour interval is 2 ^{o}C with 10 ^{o}C and 20 ^{o}C thickened) surface wind (vector, m s^{-1}) and precipitation (white contours for the range over 3 mm day^{-1} at every 1 mm day^{-1} with 5 and 10 mm day^{-1} thickened).

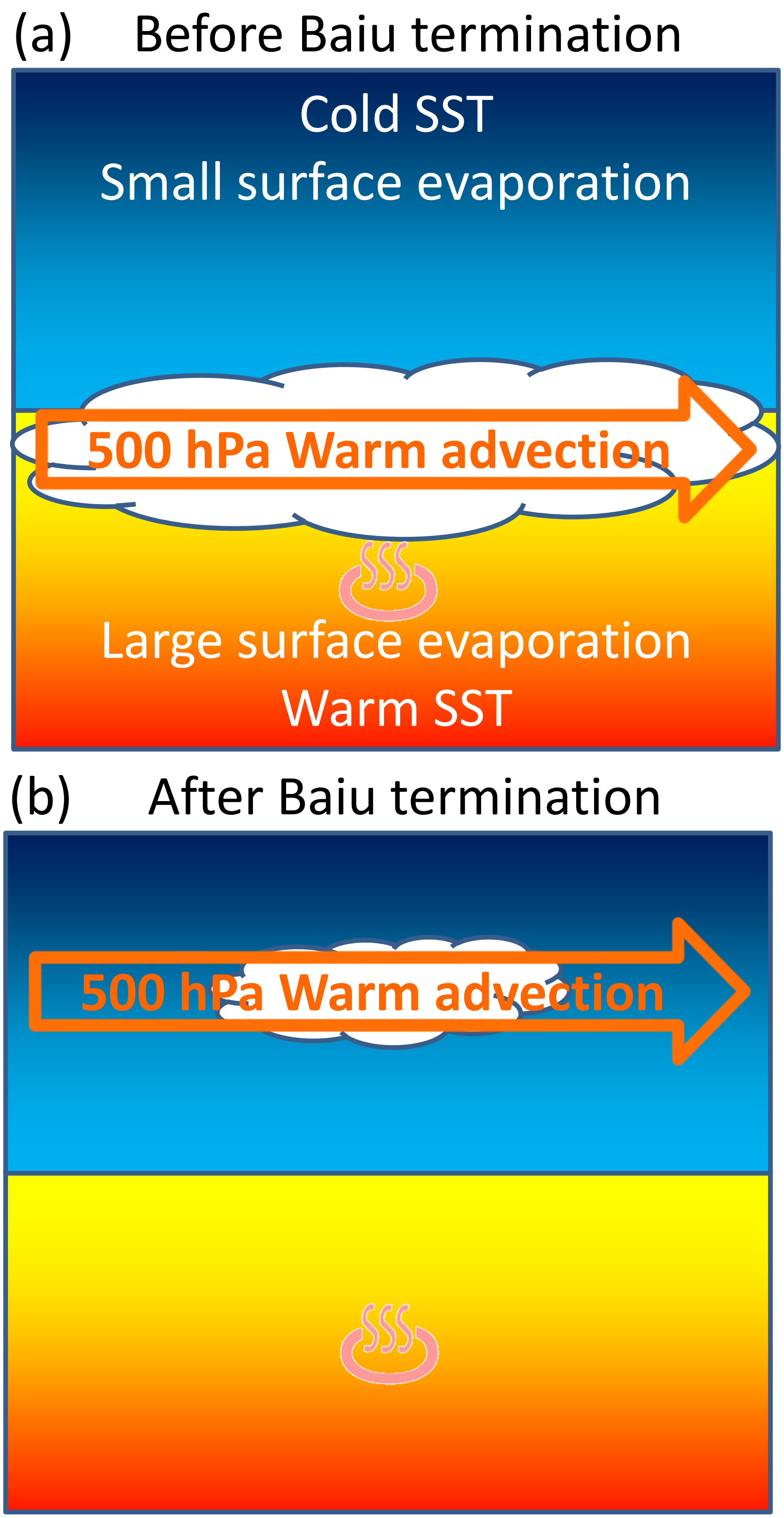

FIG. 12. A revised conceptual model of Baiu: (a) before Baiu termination and (b) after Baiu termination.